NOISE DUE TO ROTOR-TURBULENCE INTERACTION

R. K. Amiet
United Technologies Research Center

SUMMARY

A procedure for calculating the noise due to turbulent inflow to a propeller or helicopter rotor in hover is summarized. The method is based on a calculation of noise produced by an airfoil moving in rectilinear motion through turbulence. At high frequency the predicted spectrum is broadband, while at low frequency the spectrum is peaked around multiples of blade passage frequency. This paper provides the results of a parametric study of the variation of the noise with rotor tip speed, blade number, chord, turbulence scale and directivity angle. A comparison of the theory with preliminary experimental measurements shows good agreement.

INTRODUCTION

One of the potential sources of both rotor harmonic noise and broadband noise is that due to inflow turbulence. The turbulent velocity field produces a fluctuating angle of attack of the rotor blade leading to unsteady blade loading and the production of noise. If the axial length scale of the turbulence is such that a given eddy is chopped by more than one blade, the noise will tend to concentrate around multiples of blade passage frequency, while if a given eddy is chopped only once, there is no blade-to-blade correlation and the noise is broadband.

The most rigorous method of treating this problem is to combine a model of the turbulence spectrum with airfoil response functions to determine the airfoil loading and an acoustical theory to determine the subsequent noise field. This is the approach used in references 1-3; the present study gives extensions and further results of the analysis presented in reference 1. This analysis is in turn an extension of the analysis given in reference 4 for an airfoil in rectilinear motion through turbulence which has been verified by extensive comparison with experiment in reference 5.

The basis for the extension of the rectilinear motion theory to rotational motion is that so long as the acoustic frequency is somewhat greater than the rotational frequency of the rotor, the effects of rotation can be ignored and

the blade treated as being in rectilinear motion at each instant of time. The sound can then be calculated by averaging the calculated instantaneous spectrum for one revolution of the rotor. This is described more completely in reference 1. The present analysis treats the case of helicopter hover, vertical ascent or propeller forward flight with an axial velocity. An extension to the case of helicopter forward flight is expected to be completed in the near future.

A preliminary comparison of experiment and theory shows excellent agreement between the two for the case of a model rotor with nonzero axial flow. Further comparisons between theory and experiment are presently being made.

A recent review of this and other helicopter noise sources is given in the paper by George (ref. 6).

SYMBOLS

B	Blade number
b	Blade semichord
c	Blade chord
c_o	Sound speed
d	Blade semispan
E	Acoustic energy in a harmonic peak
E(k)	Energy spectrum of turbulence
f	Acoustic frequency
g	Airfoil response function
G	Integrated airfoil response
K_x, K_y	Chordwise turbulence wavenumber and spanwise turbulence wavenumber
$\bar{k}$	$\omega b/V_\gamma$
k_e	Wavenumber range of energy-containing eddies
$\bar{k}_o$	Value of $\bar{k}$ for f = 1 Hz and $M_\gamma = 0.628$

L	Turbulence integral scale
ℓ	Effective lift
M_γ, M_z, M_r	Azimuthal, axial and relative blade Mach numbers
ΔP	Pressure jump on airfoil
R	Effective radius of rotor
r	Distance to observer
RPS	Revolutions per second
S_{pp}	Acoustic spectrum
$S_{pp_{max}}$	Maximum spectrum level of a harmonic peak
s	Rotor span
T	Blade passage time
t	Time
$\overline{u^2}$	Mean square turbulence velocity
V_γ, V_z, V_r	Azimuthal, axial and relative rotor velocities
w_o	Unsteady velocity normal to rotor blade
$\underline{X}$	Vector position of observer
x,y,z	Cartesian coordinate system fixed to rotor hub; nonrotating
x',y',z'	Cartesian coordinate system; y' along rotor span; x' along chord
γ	Azimuthal angle
Γ	Gamma function
θ	Angle of observer from rotor axis
λ	Acoustic wavelength
ρ_o	Density

Φ_{ww}	Turbulence spectrum
ω	Radian frequency of blade forces
ω_o	Doppler shifted frequency heard by observer

THEORETICAL FORMULATION

Notation and Summary of Analytical Method

The geometry for the problem is given in figure 1 and is the same as that of reference 1. The rotor blade is divided into segments and the noise contribution of each segment is calculated. The relative velocity V_r of a blade segment is related to the azimuthal velocity V_γ and the axial velocity V_Z by

$$V_r^2 = V_\gamma^2 + V_Z^2 \tag{1}$$

The basis for the analytical method is to utilize a noise calculation procedure for an airfoil in rectilinear motion through turbulence (see refs. 4-5). This calculation is applied to calculate the noise produced in the far-field by a segment of the rotor span as if that segment were in rectilinear motion. This is repeated for different azimuthal rotor positions, and an average spectrum is then obtained by integrating over the azimuth, remembering to account for the differing amounts of retarded time spent by the rotor in each azimuthal location.

The final result for the far-field spectrum given in reference 1 is (note that the expression in reference 1 is for a single blade and is here multiplied by the number B of blades)

$$S_{PP}(\omega_o, \underline{X}) = \frac{V_r B}{T V_\gamma V_Z} \int_0^{2\pi} \frac{\omega}{\omega_o} G \sum_{n=-\infty}^{\infty} \Phi'_{ww}\left(K_x, K_y, \frac{V_r}{V_\gamma V_Z}(\omega_o + 2\pi n/T)\right) d\gamma \tag{2}$$

The function G represents the integrated airfoil response function and is given by

$$G \equiv \left[\frac{\omega \rho_o b z}{C_o (r + M_r x')^2}\right]^2 \pi V_r \, d \left|\mathcal{L}\right|^2 \frac{\omega}{\omega_o} \tag{3}$$

with

$$\mathcal{L} \equiv \int_{-1}^{1} g(\xi)\, e^{i\xi K_y x'/y'}\, d\xi \tag{4}$$

Without the exponential factor in equation (5), $\mathcal{L}$ would be just the airfoil lift per unit span. The exponential factor accounts for differences in propagation time to the observer from different points on the airfoil surface. Thus, $\mathcal{L}$ could be called an effective lift and it depends on observer location. A skewed gust of the form

$$w_g = w_o\, e^{i(\omega t - K_x x' - K_y y')} \tag{5}$$

produces a pressure jump distribution ΔP on the airfoil. The airfoil response function g is then defined by the normalization

$$g \equiv \Delta P\, e^{-(i\omega t - K_y y')} / (2\pi \rho_0 V_r w_o) \tag{6}$$

Analytical expressions for g can be found in references 7-8 and the evaluation $\mathcal{L}$ is discussed further in reference 1.

In equation (2), T is the blade passage time, Φ'_{ww} is the turbulence spectrum for the velocity component normal to the airfoil as written in the primed coordinate system, and K_x and K_y are the chordwise and spanwise turbulence wavenumbers. The radian sound frequency ω in an airfoil fixed frame is related to K_x by

$$K_x = \omega / V_r \tag{7}$$

The relevant K_y turbulence wavenumber is determined by the observer location; i.e.,

$$K_y = K_x\, M_r\, y'/(r + M_r\, x') \tag{8}$$

The radian frequency ω_o is the sound frequency measured in a nonrotating frame fixed to the rotor hub and so is related to ω by a Doppler factor, i.e.,

$$\frac{\omega}{\omega_o} = \frac{1 - M_z \cos\theta}{1 + M_r\, x'/r} \tag{9}$$

The airfoil semichord is b, d and s are the semispan and span, respectively, and R is the distance of the airfoil segment from the rotor axis.

Energy in an Isolated Harmonic Peak

When the harmonic narrow-band-random peaks in the spectrum are separated by deep troughs it is possible to derive a simple expression for the overall energy contained in each peak. To determine the energy in a peak, equation (2) must be integrated over ω_o between the troughs bordering the peak of interest. The peaks will be isolated (i.e., there will be a rapid drop off with ω_o on each side of a peak) if the k_z or third argument of Φ_{ww} varies rapidly enough with ω_o; more explicitly, the peaks will be isolated if

$$V_r L >> V_z V_\gamma T \tag{10}$$

where L is the turbulence integral scale. If this is the case, then the variation of K_x and K_y with ω_o can be neglected in the ω_o integral. The troughs in the sound spectrum are separated by $2\pi/T$. Thus the range of integration is ω_1 to $\omega_1 + 2\pi/T$ where ω_1 represents the trough to the left of the peak. Then noting that for any functions f(x)

$$\sum_{n=-\infty}^{\infty} \int_{x_1}^{x_1+2\pi/T} f(x + 2\pi n/T)\, dx = \int_{-\infty}^{\infty} f(x)\, dx \tag{11}$$

the energy contained in a peak is found by integration of equation (2) to be

$$E(\omega_o, \underline{X}) = \int_{\omega_1}^{\omega_1+2\pi/T} S_{PP}(\omega_o, \underline{X})\, d\omega_o \tag{12}$$

$$= \frac{B}{T} \int_0^{2\pi} \frac{\omega}{\omega_o} G(\omega) \int_{-\infty}^{\infty} \Phi'_{ww}(K_x, K_y, \xi)\, d\xi\, d\gamma$$

It will be noted that this is the same energy which would be calculated to be in the band $\omega_1 < \omega_o < \omega_1 + 2\pi/T$ if there were no blade-to-blade correlation. Thus, blade-to-blade correlation acts to concentrate the acoustic energy around multiples of blade passage frequency, but it is not basically a method

of increasing the total acoustic energy radiated (unless one considers large correlation lengths and low frequencies such that blades are simultaneously correlated so that in the far field one adds pressures rather than intensities).

For an observer on the centerline, a simple result can be obtained for the ratio of the sound energy in a discrete harmonic peak to the maximum peak level. For an observer on the propeller axis the γ integration in equation (2) simply introduces the factor 2π. At a blade passing harmonic, ω_o will be some multiple of $2\pi/T$. Since the harmonic peaks are widely separated, then using equation (10) it can be seen that only the first term in the sum is needed. The maximum at a peak is then

$$S_{PP_{max}}(\omega_o, z) = \frac{2\pi B G V_r}{T V_\gamma V_z} \Phi'_{ww}(K_x, 0, 0) \tag{13}$$

In this equation, the parameter ω to be used in G, K_x and K_y is equal to ω_o as expected since there is no Doppler shift for an observer on the centerline. This can be seen also from equation (9) by noting that

$$x' = \frac{1}{V_r}\left[V_\gamma(x \sin\gamma - y\cos\gamma) - V_z z\right]$$

which becomes $x' = -V_z z/V_r$ for an observer on the z axis. Likewise, for an observer on the z axis, equation (12) for the energy in a peak becomes

$$E(\omega_o, z) = 2\pi \frac{B}{T} G \int_{-\infty}^{\infty} \Phi'_{ww}(K_x, 0, k_z)\, dk_z \tag{14}$$

Taking the ratio of equations (13) and (14) gives

$$\frac{E}{S_{PP_{max}}} = \frac{V_\gamma V_z}{V_r} \int_{-\infty}^{\infty} \frac{\Phi'_{ww}(K_x, 0, k_z)}{\Phi'_{ww}(K_x, 0, 0)}\, dk_z \tag{15}$$

Introducing the Kármán spectrum function

$$\Phi_{ww}(k_x, k_y, k_z) = \frac{E(k)}{4\pi k^2}\left(1 - k_z^2/k^2\right)$$

$$E(k) = \frac{I k^4}{\left[1 + (k/k_e)^2\right]^{17/6}}$$

$$k^2 = k_x^2 + k_y^2 + k_z^2$$

$$I = \frac{55}{9\sqrt{\pi}} \frac{\Gamma(5/6)}{\Gamma(1/3)} \frac{\overline{u^2}}{k_e^5} \qquad (16)$$

$$k_e = \frac{\sqrt{\pi}}{L} \frac{\Gamma(5/6)}{\Gamma(1/3)}$$

allows the integral in equation (15) to be calculated giving

$$\frac{E}{S_{PP_{max}}} = \frac{16\pi}{55} \frac{V_y V_z}{V_r L} \sqrt{1 + K_x^2/k_e^2} \qquad (17)$$

This should be a useful result for calculating the overall intensity at a given directivity location. Strictly speaking it is only valid for an observer on the rotor axis, but it should provide meaningful estimates for other observer positions.

CALCULATED RESULTS

Several calculated spectra will be presented here for the purpose of illustrating the type of results expected, and for determining the dependence on the various parameters of the problem. In reference 1 it was shown that the results obtained by placing the entire span at an effective radius, R, equal to 0.8 of the tip radius were not significantly different from the results obtained by integration over the blade span. Thus, the present calculations will use the effective radius approach. For the calculations presented here, unless specified otherwise, the following input parameters to the calculation will be assumed.

R/c	= 10	M_z	= 0.1
s/c	= 10	B	= 2
r/c	= 100	$(\overline{u^2}/V_z^2)^{1/2}$	= 0.01
c_o/c	= 1000	RPS	= 10
L/c	= 100	θ	= 0

Figure 2 shows the effect of tip Mach number on the noise. At low frequencies, harmonics of blade passage frequency begin to stand out as shown by the dashed lines. In subsequent figures only the envelope of the peaks and troughs will be shown. The abscissa is a reduced frequency, $\overline{k} = \omega b/V_\gamma$, normalized by a reference value $\overline{k}_o$ which is the value of $\overline{k}$ for f = 1 Hz and $M_\gamma = 0.628$. Thus, since the smaller of the two tip velocity cases is half of the higher one, a given value of frequency for the smaller V_γ case occurs at an abscissa which is twice the value for the large V_γ case. The reason for normalizing the frequency abscissa in this manner is so that for a given abscissa value, both cases will show the results of an interaction with the same turbulence wavenumber component. In other words, for a given turbulence component, as the blade velocity is increased, the frequency of the sound produced will increase.

Dipole noise is commonly associated with a V^6 velocity dependence. However, this is based on certain assumptions which do not hold for the present problem, e.g., the turbulence intensity is here assumed to remain fixed as the rotor velocity increases, rather than increasing proportional to the rotor speed. In discussing the velocity dependence of the spectrum, the high frequency and the low frequency portion of the curve will be discussed separately.

For high frequency and for V_r not too near 1, $|\mathcal{L}|^2$ behaves as $1/V_r$ for fixed $\overline{k}$. Thus, for large ω and fixed $\overline{k}$, G varies approximately as V_r^2 for an on-axis observer. For large ω the summation in equation (2) can be replaced by an integral over k_z, bringing the factor $V_z V_\gamma T/(2\pi V_r)$ out front of the integral. The final result is that the high frequency portion of the spectrum increases as V_r^2 at a given fixed $\overline{k}$. The overall energy contained in the spectrum in the range from a given $\overline{k}$ value to infinity will increase as V_r^3, however, since the plotted spectra represent the energy per unit Hertz rather than per unit $\overline{k}$ and there is a factor of 2 in the frequency ranges of the two curves. (Added note: equation (2) represents the energy per unit ω_o, and a factor of 2π must be introduced to convert it to a per Hertz basis. The plotted spectra are on a per Hertz basis.)

At low frequency $|\mathcal{L}|$ is independent of V_r. Thus, for an on-axis observer G varies as V_r^3 for fixed $\overline{k}$. The summation in equation (2) reduces to the single term $\Phi'_{ww}(K_x, 0)$ at a peak of a blade passing harmonic. For $V_z \ll V_\gamma$, $V_r \sim V_\gamma$ and the spectrum then is proportional to V_r^3/T. The variation of V_γ in figure 2 was obtained by varying the rotor rotational frequency, while that of figure 3 was obtained by varying the rotor effective radius at constant rotational frequency. Thus, T varies with V_γ in figure 2 but not in figure 3; in figure 2 the amplitude of a harmonic peak varies as V_r^4 and in figure 3 it varies as V_r^3. In calculating the overall energy, it will be noted that halving V_γ cuts the number of harmonic peaks in half. This together with the approximately 9 dB drop in the peaks gives approximately a 12 dB effect, the same as

for figure 2. Using equation (17) for the ratio of energy to harmonic peak amplitude shows that there is no additional V_r dependence so that the final velocity dependence of the energy at low frequency is V_r^4.

These results are in accord with the results for an airfoil in rectilinear motion given by equation (17) of reference 9. If the turbulence intensity had been allowed to vary with rotor velocity, the velocity dependence of the acoustic energy would have been the more familiar results V^5 and V^6 at high and low frequency, respectively.

Figures 4 and 5 show the effect of changing the number of rotor blades. At high frequency there is no blade-to-blade correlation and each rotor blade acts independently of the others. Thus, doubling B increases the noise by 3 dB. This is illustrated in figure 4 where 3 dB has been subtracted from the curve for B = 4 to illustrate that for high frequencies it then becomes coincident with the B = 2 curve. Figure 5 shows the effect on the envelope of the harmonics at low frequency. Note that the abscissa has a factor of B in it. Thus, for a given value of the abscissa, the two curves which have values of B differing by a factor of 2 will differ in frequency also by a factor of 2. Then every harmonic peak in one of the two plots will have a corresponding peak in the other plot. For this problem the first and subsequent blade passing harmonics are in the range $k >> k_e$. Equations (16) then show that $\Phi_{ww} \sim \omega^{-11/3}$. Since the reduced frequency $\bar{k}$ is small, $\mathcal{L}$ is not a strong function of ω and equation (3) shows that $G \sim \omega^2$. The frequency of any given harmonic varies as $\omega^2 \sim B/T$. Thus, from equation (13) $S_{pp_{max}} \sim \omega^{1/3}$ which is a weak dependence, and the levels of corresponding harmonics in figure 5 would be expected to be about the same. This is seen to be the case. Equation (17) then shows that the energy contained in each of the harmonics for B = 4 will be twice that for B = 2. Thus, both the low and high frequency regimes give a 3 dB effect; that is, an overall doubling of the noise for a doubling of the blade number. It should be remembered, however, that the present calculation does not include any steady loading effects on the noise. If this were important, then decreasing the steady loading by increasing the blade number could have a significantly different effect.

Figure 6 shows the effect of changes in blade chord on the noise. In equation (2) the chord appears explicitly only in the airfoil response function. When the sound wavelength becomes smaller than about 4 chords, the airfoil begins to act like an airfoil of infinite chord. Thus, changes in chord have little effect at high frequency as is noted in figure 6. For a given frequency, as the chord decreases the reduced frequency decreases to the point where eventually the airfoil is responding in a quasi-steady manner. In this regime the airfoil response is proportional to the chord, and the sound is proportional to the square of the chord. This can be seen by comparing the first harmonic of the C/10 curve (54 dB) with that of the C curve (72 dB, shown in figures 2-5);

i.e., a tenfold change in chord gives a 20 dB change in the noise at low frequency. Again it should be remembered that this ignores the effects on the other noise sources that changing the chord might have.

Figure 7 shows the effect that variation in the turbulent length scale has. From equations (16) it will be noted that for an on-axis observer when $k >> k_e$ ($10 f L >> V_r$) Φ_{ww} behaves as $L^{-2/3}$. This gives a 6.67 dB decrease for each tenfold increase in L, a relation which is seen to hold in figure 7 over most of the frequency range for all three curves. In fact, it is only below 100 Hz for the curve representing the smallest turbulence scale (L = C) that this relation does not hold.

Figure 8 shows the effect of finite Mach number on directivity. The small Mach number case given has a directivity which is nearly that of a compact dipole. The directivity is not exactly that of a dipole since the rotor blades are aligned with the relative flow, rather than lying in the plane of rotation. All the curves are normalized to 0 dB at $\theta = 0$; i.e., on the upstream axis. The directivity plots for the higher Mach number cases tend to be pushed outward toward the rotor axis for most angles when compared with the low Mach number case.

Figure 9 presents a comparison of theory with preliminary experimental results. The experiment was performed in the UTRC open-jet Acoustic Research Tunnel. The turbulence was generated by an upstream grid as in reference 5, and measurements verified that the turbulence was essentially isotropic. The experimental results are presented "as measured," while the theoretical results include a correction to account for the presence of the tunnel open-jet shear layer through which the sound must pass before reaching the observer. It should be emphasized that there were no adjustable parameters in the theory which could be used to improve agreement between theory and experiment. The turbulence length scale and intensity were measured independently of the acoustic test. The large peak at blade-passage-frequency is due to the steady blade loading. Other than this steady loading effect which is not included in the present formulation, the agreement between theory and experiment appears accurate to within a few dB. Additional experiments are presently in progress to give further assessment of the theory.

CONCLUDING REMARKS

The change in the noise produced by a variation of the parameters affecting turbulence ingestion noise can be summarized as follows for an observer on the axis of the rotor:

(1) The acoustic energy has a V_γ^4 dependence at low frequency and a V_γ^3 dependence at high frequency.

(2) The acoustic energy increases linearly with blade number at high frequency and nearly linearly at low frequency.

(3) The effect of blade chord on noise is small for wavelengths greater than about 4 chords. For chords small compared to the wavelength, the noise is proportional to the square of the chord.

(4) The noise spectrum varies with the -2/3 power of the turbulence integral scale except when L is comparable to or less than the chord and the frequency is low.

(5) The directivity plots tend to be flattened toward the rotor plane when the Mach number is significant.

The most effective method of reducing the noise appears to be through reduction of blade tip speed because of the rather strong velocity dependence of the noise, although not as strong as V^6 which one often expects for dipole noise. In lowering the tip velocity, other parameters would also have to be changed to maintain rotor thrust, and this could offset somewhat the beneficial effect of a decrease in tip speed.

A comparison with preliminary experimental results gives strong support to the theory. A more comprehensive experimental assessment of theory is currently in progress. These experiments include the case of simulated forward flight in which the ambient flow is not axial. The present theory is being extended to treat this case. Also, although the calculations performed here were for the case of isotropic turbulence, the case of anisotropic turbulence can be treated if a satisfactory model of the turbulence spectrum is available.

REFERENCES

1. Amiet, R. K.: Noise Produced by Turbulent Flow into a Propeller or Helicopter Rotor. AIAA Paper no. 76-560, July 1976. Also AIAA Journal, vol. 15, no. 3, March 1977, pp. 307-308.

2. Homicz, G. F. and George, A. R.: Broadband and Discrete Frequency Radiation from Subsonic Rotors. J. Sound and Vib., vol. 36, 1974, pp. 151-177.

3. George, A. R. and Kim, Y. N.: High Frequency Broadband Rotor Noise. AIAA Journal, vol. 15, no. 4, April 1977, pp. 538-545.

4. Amiet, R. K.: Acoustic Radiation from an Airfoil in a Turbulent Stream. J. Sound and Vib., vol. 41, 1975, pp. 407-420.

5. Paterson, R. W. and Amiet, R. K.: Noise and Surface Pressure Response of an Airfoil to Incident Turbulence. J. Aircraft, vol. 14, no. 8, August 1977, pp. 729-736.

6. George, A. R.: Helicopter Noise-State of the Art. AIAA Paper no. 77-1337, October 1977.

7. Amiet, R. K.: Compressibility Effects in Unsteady Thin-Airfoil Theory. AIAA Journal, vol. 12, February 1974, pp. 252-255.

8. Amiet, R. K.: High Frequency Thin Airfoil Theory for Subsonic Flow. AIAA Journal, vol. 14, August 1976, pp. 1076-1082.

9. Paterson, R. W. and Amiet, R. K.: Acoustic Radiation and Surface Pressure Characteristics of an Airfoil Due to Incident Turbulence. NASA CR-2733, 1976.

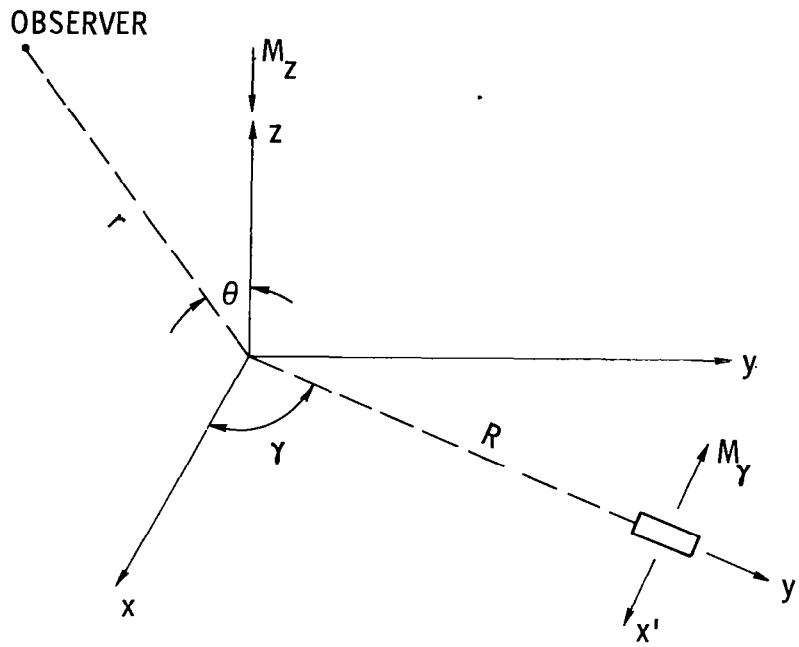

Figure 1.- Geometry for rotating blade segment.

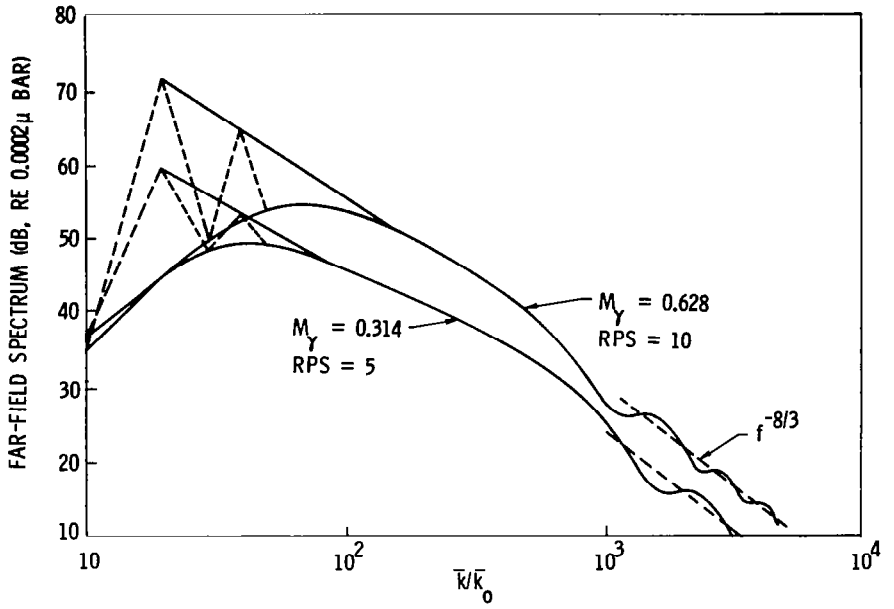

Figure 2.- Effect of tip Mach number on spectrum; variation of rotational frequency.

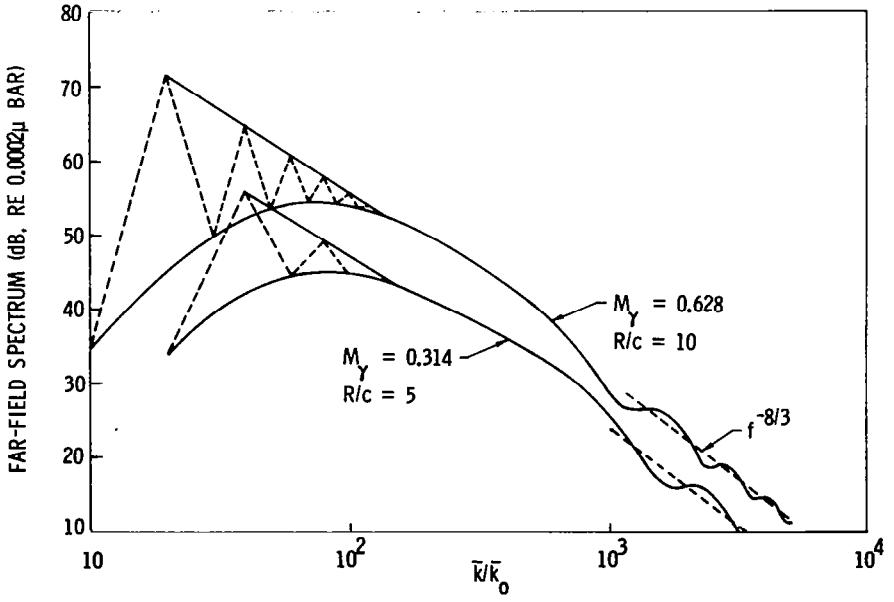

Figure 3.- Effect of tip Mach number on spectrum; variation of effective blade radius.

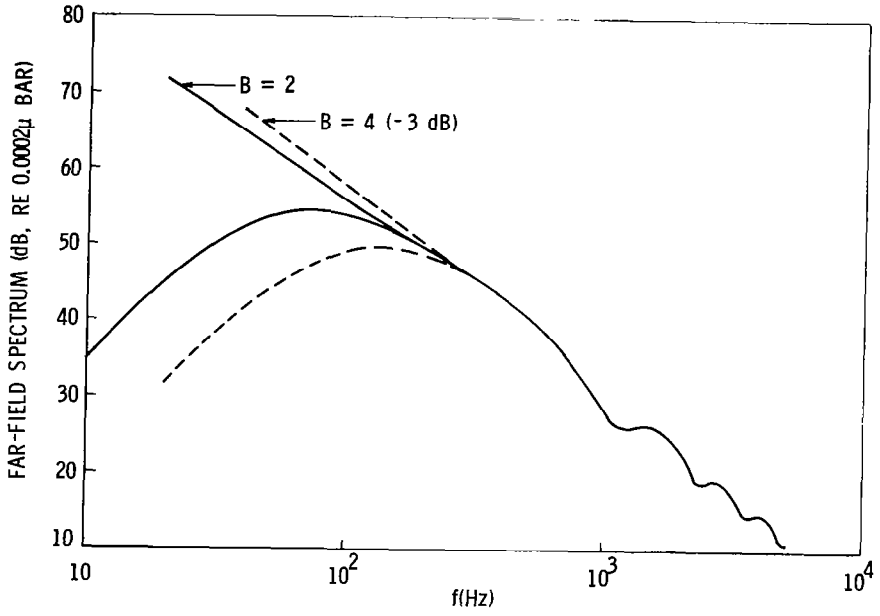

Figure 4.- Effect of blade number on spectrum.

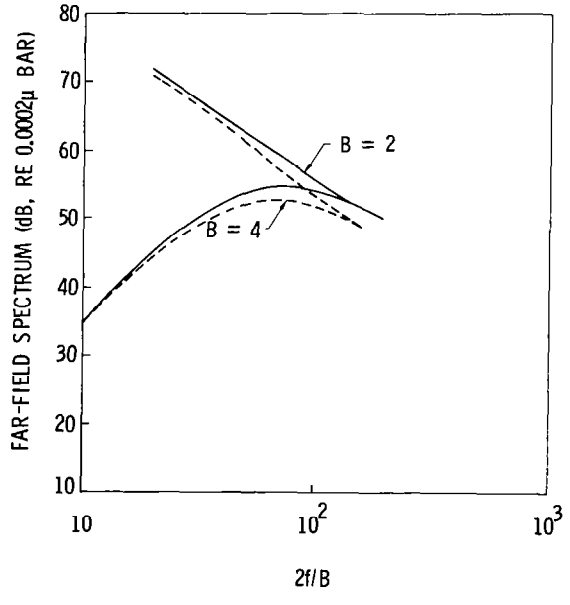

Figure 5.- Effect of blade number on low frequency spectrum.

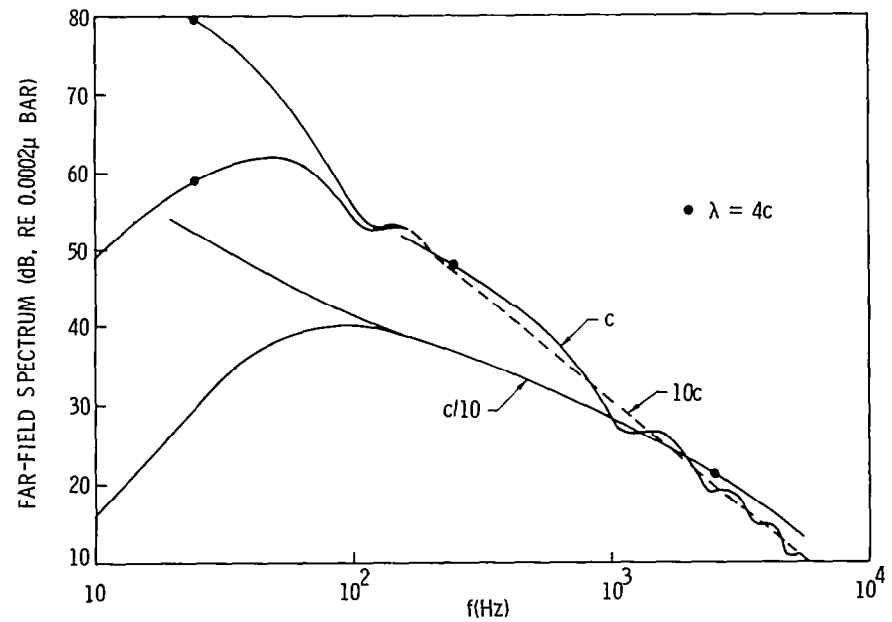

Figure 6.- Effect of blade chord on spectrum.

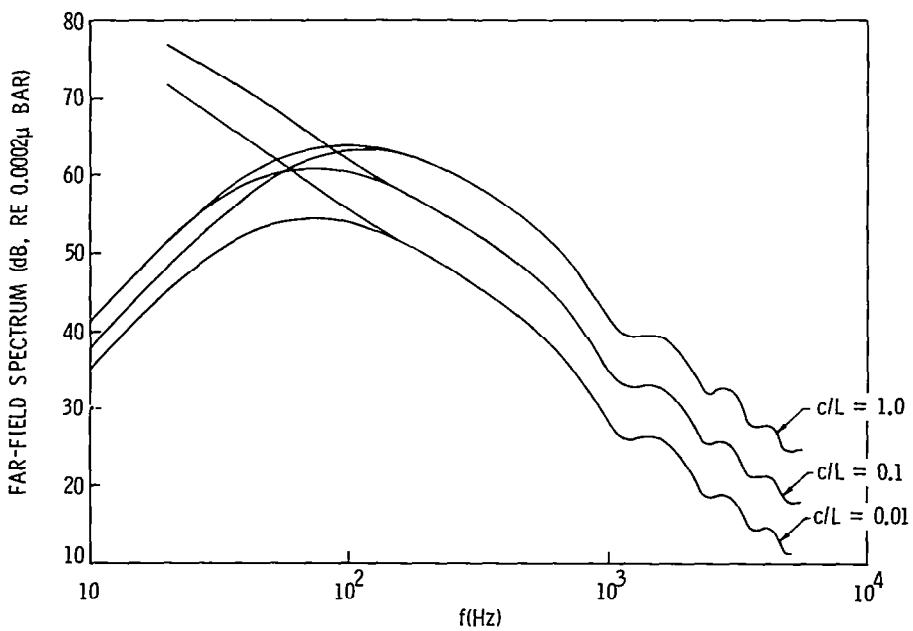

Figure 7.- Effect of turbulence length scale on spectrum.

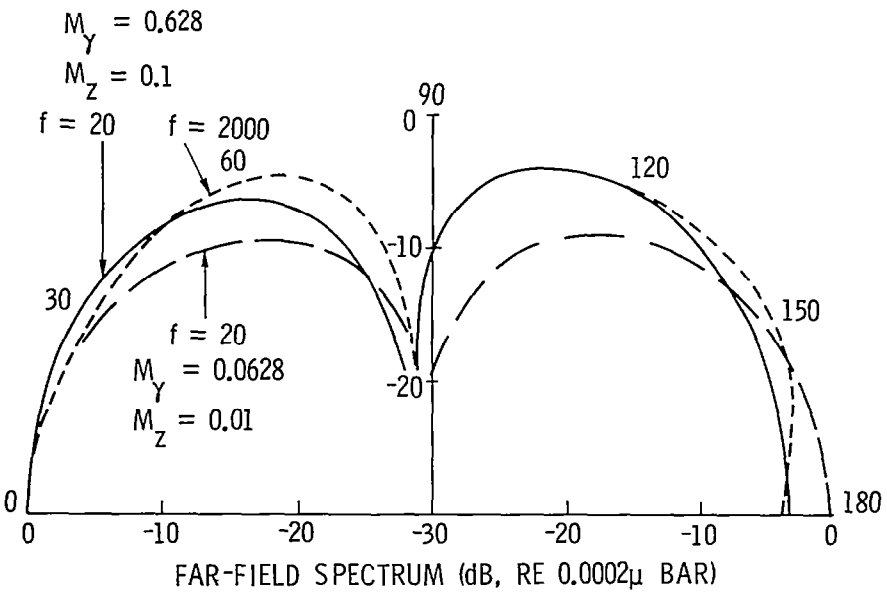

Figure 8.- Effect of tip Mach number on directivity.

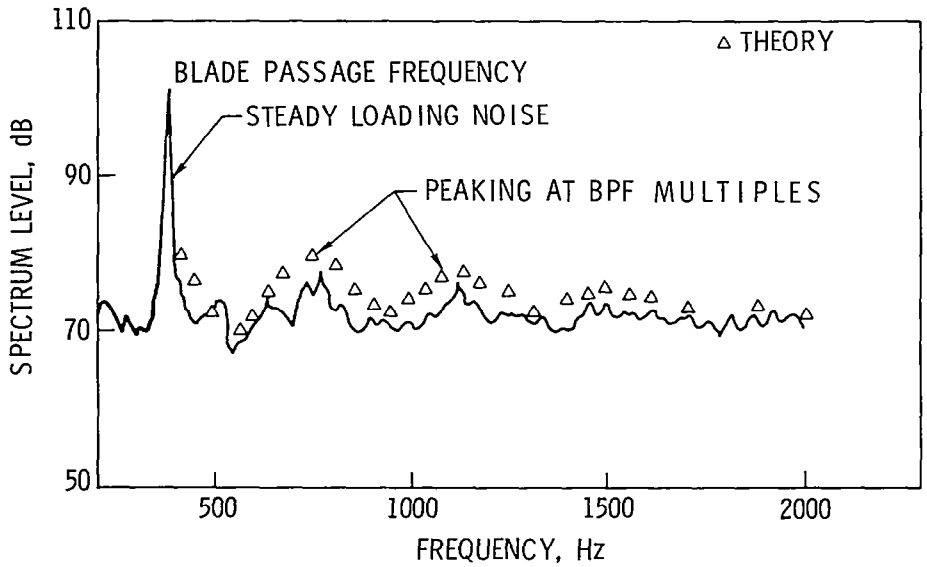

Figure 9.- Comparison of theory and experiment. M_z = 0.097; M_Y = 0.418; c/L = 1.1842; B = 4, c_o/c = 6022.5; $(\overline{u^2/V_z^2})^{1/2}$ = 0.067; R/c = 4.3; r/c = 4.3; r/c = 53.3; s/c = 5.33; RPS = 94.0; θ = 124.85.